JOURNAL OF MATERIALS SCIENCE 20 (1985) 1514–1520

An elastodynamic fracture analysis in a centre-cracked plate

M. PERL
Faculty of Mechanical Engineering, Technion-Israel Institute of Technology, Haifa–32000, Israel

A two-dimensional linear elastodynamic analysis of crack initiation and fast crack propagation in a centre-cracked plate, subjected to constant tension is presented. The analysis is performed using the previously developed SMF2D code in its generation mode. The experimentally measured crack tip motion, as well as the specimen's geometry and its material characteristics serve as input to the simulation. The dynamic stress intensity factor, the dynamic energy release rate, and the various energy distributions are subsequently evaluated. Special attention is given to the influence of the energy supplied to the body during the fracture process due to the work done by the external tractions.

1. Introduction

Preliminary results regarding crack initiation and dynamic crack propagation in a centre-cracked plate (CCP), using the improved two-dimensional finite difference code, the SMF2D code, were reported by Perl *et al.* [1]. Using generation phase type simulations, the influence of the initial crack length and the initial loading (bluntness) on the various dynamic parameters of the problem is investigated in this paper. In each case discussed, the crack tip motion is specified using experimental data and the dynamic parameters such as the dynamic stress intensity factor, the dynamic energy release rate, and the various energy distributions are evaluated throughout the simulation.

In the following sections, after a brief description of the field equations and the numerical scheme, detailed static and dynamic results for the CCP specimen are presented and discussed. Furthermore, a comprehensive comparison between the CCP and the single edge notch specimen (SEN), under fixed grip conditions, is performed.

2. The field equations

Only a brief description of the field equations and the numerical scheme is hereafter given. A detailed description of the employed method, the numerical approximation as well as the SMF2D code are given in [1–3].

The SMF2D code is based on the simultaneous employment of two coordinate systems (Fig. 1). The stationary coordinate system which is attached to the treated body, defining the stationary domain D_s, and the moving coordinate system which originates at the moving crack tip, defining the moving domain D_m.

Assuming an elastic medium under plane strain conditions, the dimensionless displacement field U in the stationary domain D_s is governed by the following equations of motion:

$$\frac{1}{2(1-\nu)}[U_{k,ki} + (1-2\nu)U_{i,kk}] = U_{i,\tau\tau} + \psi U_{i,\tau} \qquad i,k = 1,2 \tag{1}$$

Here U was normalized to an arbitrary unit of length, H, say for convenience the height of the specimen investigated. The dimensionless time τ was normalized to H/C_1 where C_1 is the dilatational or the plate wave velocity depending upon whether plane strain or plane stress conditions prevail. ν is the Poisson's ratio of the material investigated, but it is replaced by the apparent ratio $\nu^* = \nu/(1+\nu)$ in plane stress conditions. The last term in Equation 1 has been added for solving the static case using dynamic relaxation [4]. ψ is a parameter by which the code is switched from the static case ($\psi > 0$) to the dynamic one ($\psi = 0$). Equation 1 together with the appropriate

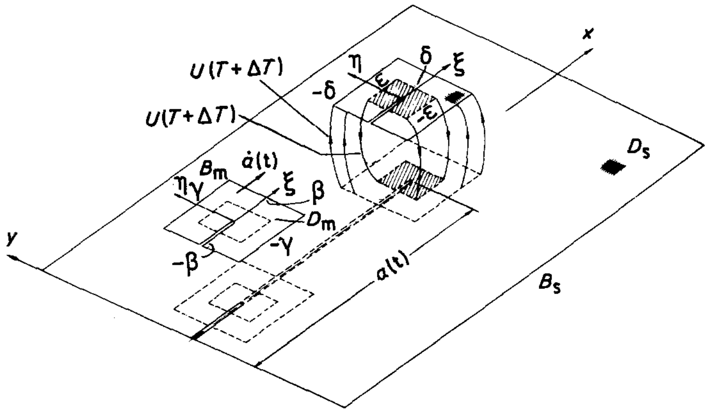

Figure 1 The stationary and the moving grids.

boundary conditions for the particular problem being solved [2] completely define the problem in the stationary domain.

The moving coordinate system being attached to the moving crack tip satisfies the relation:

$$\xi = x - \alpha(\tau)$$
$$\eta = y \tag{2}$$

where $\alpha(\tau)$ is the non-dimensional time dependent crack length. Therefore, in the moving domain D_m the equations of motion (Equation 1) being expressed in terms of ξ and η become:

$$\frac{1}{2(1-\nu)}\left[U_{k,ki} + (1-2\nu)U_{i,kk}\right] = U_{i,\tau\tau} - 2\dot{\alpha}(\tau)U_{i,1\tau} + [\dot{\alpha}(\tau)]^2 U_{i,11} - \ddot{\alpha}(\tau)U_{i,1} + \psi U_{i,\tau}$$
$$i,k = 1,2 \tag{3}$$

where the dot denotes differentiation with respect to time. The only boundary condition which applies to the moving domain is the traction free surface of the crack:

$$\sigma_{\eta\eta} = \sigma_{\xi\eta} = 0 \text{ on } \eta = 0 \text{ for } -\beta \leqslant \xi < 0 \tag{4}$$

where: σ_{ij} = the stress tensor components.

The field equations for both the stationary and the moving domains (Equations 1 and 3) subjected to the appropriate boundary conditions are solved by the finite difference method. The equations and the boundary conditions are approximated by finite differences to a second order accuracy thus yielding an explicit three level time-step algorithm for solving the static and the dynamic displacement fields.

The two main variables evaluated during dynamic as well as during static simulations, are the stress intensity factor K_I^{dyn} or K_I^{stat}, and the energy release rate G_I^{dyn} and G_I^{stat} calculated from the U field on D_m. The cleavage stress $\sigma_{\eta\eta}(\tau)$ at the mesh point lying on $\eta = 0$ next to the crack tip normalized to $\sigma_{\eta\eta}(0)$ at initiation, serves as a measure of the dynamic stress intensity factor K_I^{dyn} as compared with its static value K_I^{stat}:

$$\frac{\sigma_{\eta\eta}(\tau)}{\sigma_{\eta\eta}(0)} = \frac{K_I^{dyn}}{K_I^{stat}} \tag{5}$$

The moving domain D_m serves as a "control volume" for the evaluation of the energy release rate. $G_I^{dyn}(\tau)$ is calculated using the following equation:

$$G_I^{dyn}(\tau) = \frac{1}{\dot{\alpha}(\tau)}\left[-\frac{\partial}{\partial\tau}\int_{D_m}(e_s + e_k)\mathrm{d}\xi\mathrm{d}\eta + \oint_{B_m} T\frac{\partial U}{\partial \tau}\mathrm{d}S\right] + \oint_{B_m}(e_s + e_k)\,\mathrm{d}\eta - \oint_{B_m} T\frac{\partial U}{\partial \xi}\,\mathrm{d}S \tag{6}$$

where: e_s is the strain energy; e_k is the kinetic energy; T is the traction vector; and S is the curve length along B_m. Note that in the static case ($e_k = \partial/\partial\tau = 0$) the righthand side of Equation 6 reduces to the path independent J-integral.

As mentioned before, a detailed description of the exact treatment of the equations and the integration procedure is given in [1–3].

3. The mathematical model

The CCP specimen described in Fig. 2 is rectangular ($2H \times 2W$) and has an initial crack of $2a_0$. At its ends ED and FC the specimen is subjected to a uniform tensile stress σ_∞ acting perpendicularly to the crack's plane. Since the specimen has two

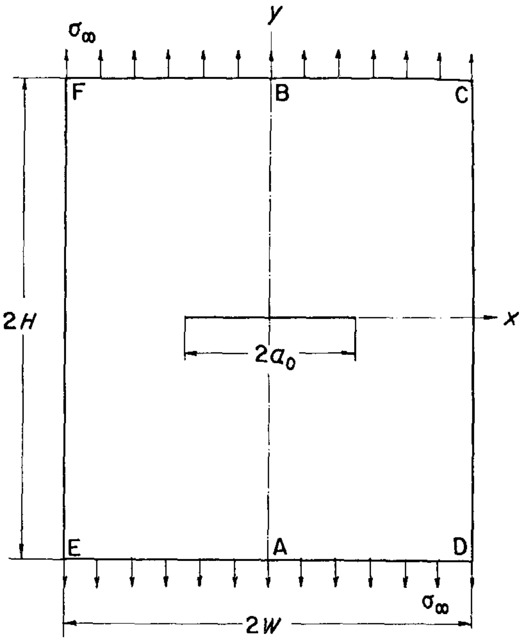

Figure 2 The centre-cracked plate.

axis of symmetry only the upper right quarter is considered ($x \geqslant 0, y \geqslant 0$), provided the boundary conditions for that part, i.e.

$$\sigma_{yy} = \sigma_{xy} = 0 \quad \text{on } y = 0 \quad \text{for } 0 \leqslant x < a_0 \tag{7a}$$

$$\sigma_{xx} = \sigma_{xy} = 0 \quad \text{on } x = W \quad \text{for } 0 \leqslant y \leqslant H \tag{7b}$$

$$\sigma_{yy} = \sigma_\infty;\ \sigma_{xy} = 0 \quad \text{on } y = H \quad \text{for } 0 \leqslant x \leqslant W \tag{7c}$$

are supplemented by the symmetry conditions:

$$U_y = \tau_{xy} = 0 \quad \text{on } y = 0 \ \text{for } a_0 \leqslant x \leqslant W \tag{7d}$$

$$U_x = \tau_{xy} = 0 \quad \text{on } x = 0 \ \text{for } 0 \leqslant y \leqslant H \tag{7e}$$

Equation 1 together with the boundary conditions (Equations 7a to e) and Equation 3 together with Equation 4 define the problem completely. Bearing in mind that the available experimental data does not supply enough information so as to be compared to numerical findings, the various parameters of the specimen were chosen to enable at least a qualitative comparison with the SEN specimen [5]. Thus, the specimen was assumed to be under plane stress, to be made of PMMA with a Poisson's Ratio of $\nu = 0.395$, and to have a height to width ratio of $W/H = 1$.

TABLE I The static results for the CCP specimen

	a_0/W	J	$K_I^{stat} = (JE)^{1/2}$	K_I^{stat}/K_I ([6])
1	0.107	0.325 21	0.502 52	0.87
2	0.2	0.733 07	0.754 23	0.90
3	0.3	1.301 44	1.004 95	0.92
4	0.4	2.107 37	1.278 80	0.95
5	0.6	5.310 95	2.030 10	1.00
6	0.8	7.807 16	2.461 37	–

In order to maintain the same accuracy as in [5] the same mesh size of $h = H/75$ was employed. Hence, the model consists of 5929 mesh points. The dynamic domain contains 140 mesh points originating from a 10×14 net.

4. The static case

In order to provide the initial conditions for the dynamic case, as well as to assess the validity and the accuracy of the numerical scheme, the static problem was solved for six crack lengths: $a_0/W = 0.107$, 0.2, 0.3, 0.4, 0.6 and 0.8. The static stress intensity factors K_I^{stat} was evaluated by means of the J-integral and the following relation:

$$K_I^{stat} = (JE)^{1/2} \tag{8}$$

Equation 8 refers to the plane stress condition; E denotes Young's modulus. The numerical results are given in Table I. Good agreement is found between the numerical results and the analytical ones given by Isida [6]. The numerical static curve is given by a dashed line in Fig. 3.

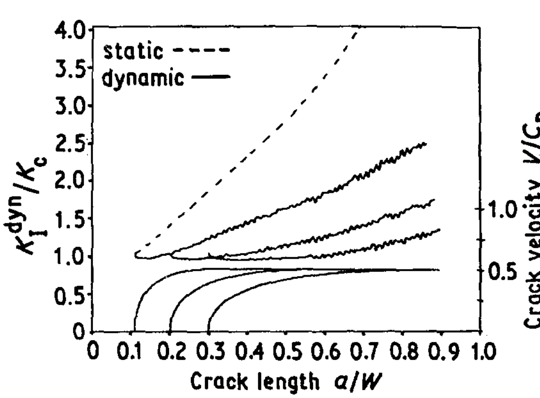

Figure 3 The normalized dynamic and static stress intensity factor for three initial crack lengths $a_0/w = 0.107$, 0.2 and 0.3.

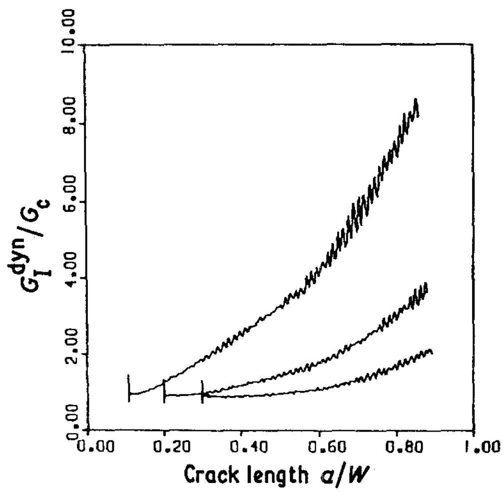

Figure 4 The normalized dynamic energy release rate for three initial crack lengths $a_0/w = 0.107, 0.2$ and 0.3.

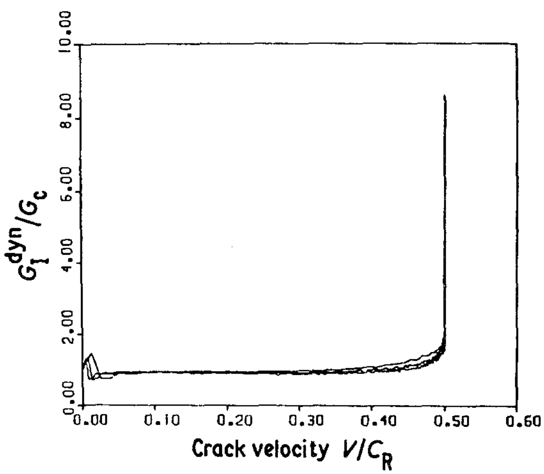

Figure 6 The dynamic energy release rate against velocity for three initial crack lengths $a_0/w = 0.107, 0.2$ and 0.3.

5. The dynamic case

In order to enable a comparison between the CCP and the SEN specimens under dynamic fracture the same procedure used for the SEN specimen as specified in [5] was adopted. Two groups of simulations were run to evaluate the influence of the initial crack length a_0/W and the initial loading. Only one of the moving crack tips in the CCP specimen will be hereafter considered.

5.1. The influence of the initial crack length a_0/W

The first three simulations were run with different initial crack lengths of $a_0/W = 0.107$, 0.2 and 0.3. The crack velocity functions were identical to those used for the SEN [5] namely, the crack was accelerated to its terminal velocity of $0.5C_R$, where C_R is the Rayleigh wave velocity while the crack extended to $3.2\,a_0/W$. This approximation is experimentally justified (see Kobayashi *et al.* [7]). K_I^{dyn}/K_c and G_I^{dyn}/G_c as functions of crack length are given in Figs. 3 and 4, and as functions of crack velocity in Figs. 5 and 6 (K_c represents the material toughness at initiation under the prevailing plane stress conditions; and $G_c = K_c^2/E$). The distribution of the strain energy U, the kinetic energy T, the fracture energy F, the external work W, and the total energy E are given in Fig. 7. In view of the above results the following conclusions can be drawn:

(a) The smaller the initial crack length a_0/W, the higher the K_I^{dyn} and G_I^{dyn} values are encountered. A similar result was found for the SEN.

(b) K_I^{dyn} and G_I^{dyn} are crack-velocity independent up to a velocity of about $0.45C_R$ after which they become highly dependent on this parameter. This is consistent with a similar finding for the SEN specimen as well as with the experimental measurements by Green *et al.* [8].

(c) During most of the crack propagation, apart from the initial zone within which the infinite body effect prevails [9], K_I^{dyn} and G_I^{dyn} are proportional to the remote stress σ_∞ and its square respectively.

(d) The total fracture energy F, sunk at the crack tip, is proportional to σ_∞^2.

(e) As in the case of the SEN specimen, K_I^{dyn} and G_I^{dyn} reach a minimum value of $0.9\,K_c$ and $0.86\,G_c$ respectively, at the end of the infinite-body-effect zone.

(f) During the initial stage of cracking the energy distributions are similar to those found in

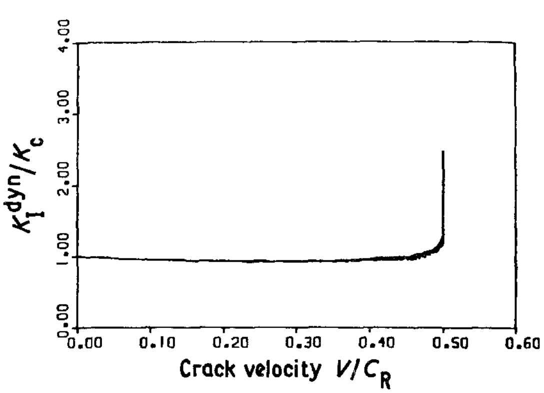

Figure 5 The dynamic stress intensity factor against velocity for three initial crack lengths $a_0/w = 0.107$, 0.2 and 0.3.

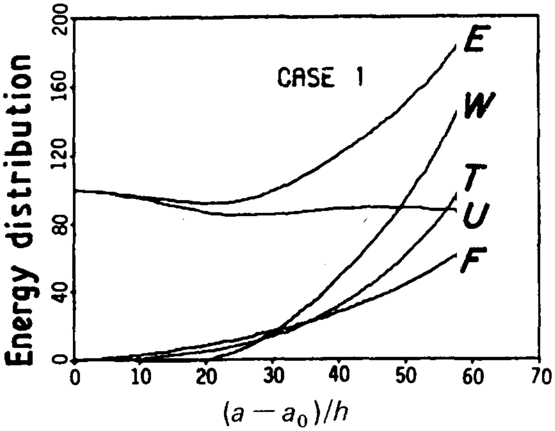

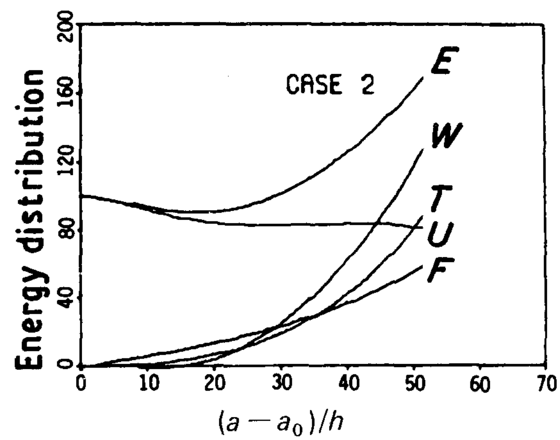

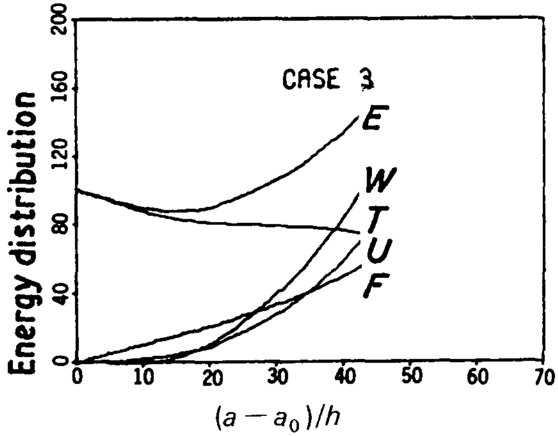

Figure 7 The energy distribution in the specimen.

the SEN specimen. Once the first dilatational wave emitted at the crack tip at initiation reaches the loaded surfaces, the external tractions start carrying out the work W on the body. This work, being accumulated by the body, changes the other energy distributions. While in the SEN specimen the conversion of strain energy into kinetic and fracture energy continues, in the CCP specimen the strain energy remains almost constant, and the further demand for the fracture energy as well as the build up of the kinetic energy is supplied by the external work W.

5.2. The influence of the initial loading K_{Iq}

Experimental results indicate that regardless of the initial loading, K_{Iq}, applied to the CCP specimen, all cracks will accelerate to one terminal velocity of about $0.5\,C_R$. Nevertheless, the higher K_{Iq} is at initiation, the higher is the acceleration prior to the constant terminal velocity. Since no quantitative information about the relation between K_{Iq} and the acceleration is available, the same procedure as for the SEN [5] will be applied hereafter. The same three velocity functions used in the previous section are now employed to represent three different crack velocity–time his-

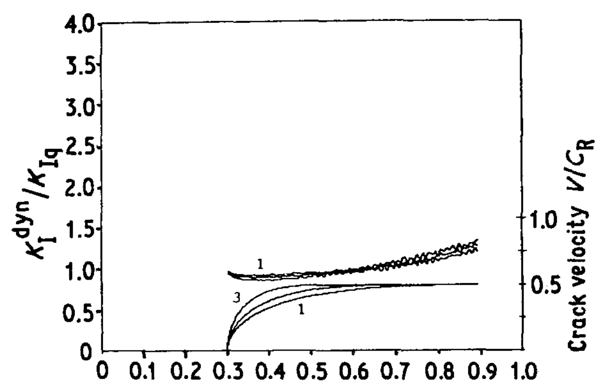

Figure 8 The dynamic stress intensity factors for three loading cases. (K_{Iq} increases from case 1 to case 3.)

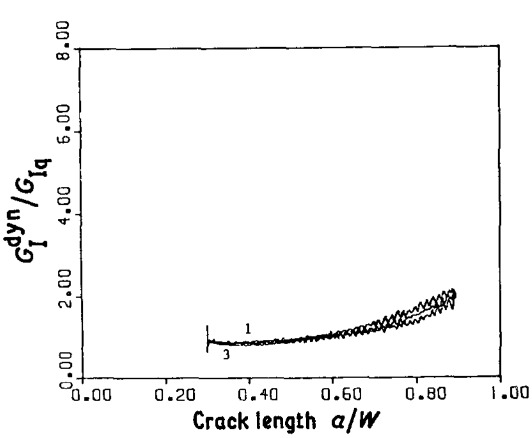

Figure 9 The dynamic energy release rates for three loading cases. (K_{Iq} increases from case 1 to case 3).

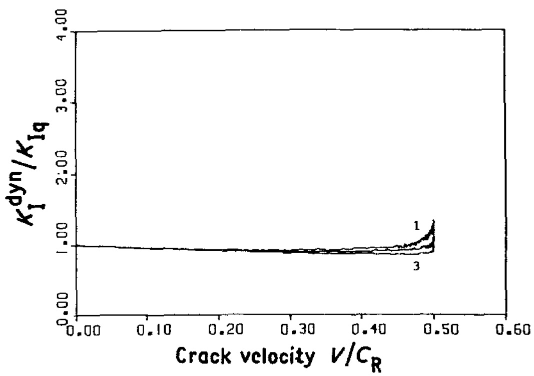

Figure 10 The dynamic stress intensity factor against velocity for three loading cases. (K_{Iq} increases from case 1 to case 3.)

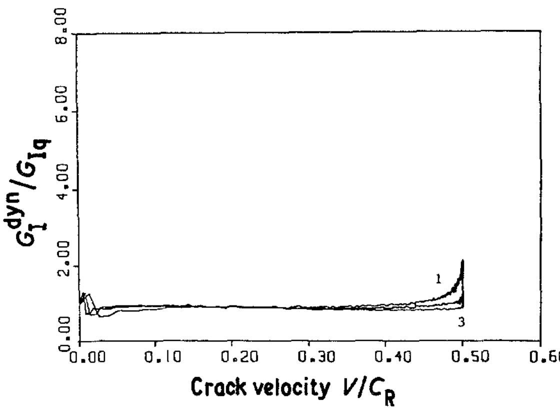

Figure 11 The dynamic energy release rate against velocity for three loading cases. (K_{Iq} increases from case 1 to case 3.)

tories for one specimen with an initial crack of $a_0/W = 0.3$ under three different loading conditions (i.e. three different K_{Iq}'s). These three velocity functions are reproduced in Fig. 8.

K_I^{dyn}/K_{Iq} and G_I^{dyn}/G_{Iq} as functions of the crack length are given in Figs. 8 and 9, and as functions of the crack velocities in Figs. 10 and 11. The various energy distributions for this case are given in Fig. 12. In view of the above results, which exhibit a similar pattern to those for the SEN specimen, the following conclusions can be made:

(a) For identical specimens with different bluntnesses, K_I^{dyn} and G_I^{dyn} are proportional to the initial loading K_{Iq} and its square respectively, throughout most of the crack propagation period, apart from the initial zone which is dominated by the infinite-body-effect.

(b) The total fracture energy is proportional to K_{Iq}^2 (see Fig. 12).

(c) The energy distributions are substantially influenced by the work done by the external tractions W (see also conclusion (f) of the previous section).

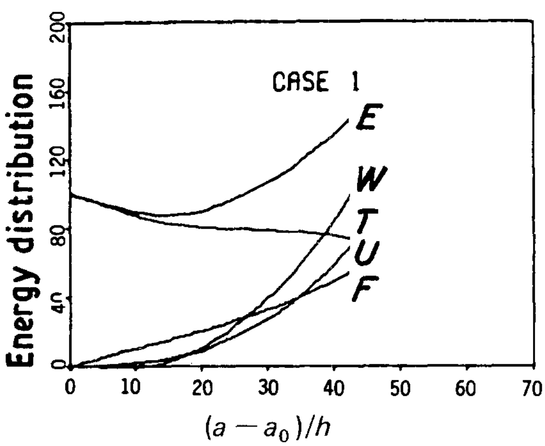

Figure 12 The energy distribution in the specimen.

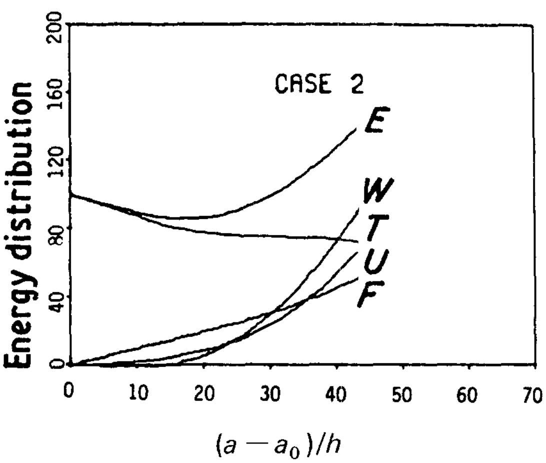

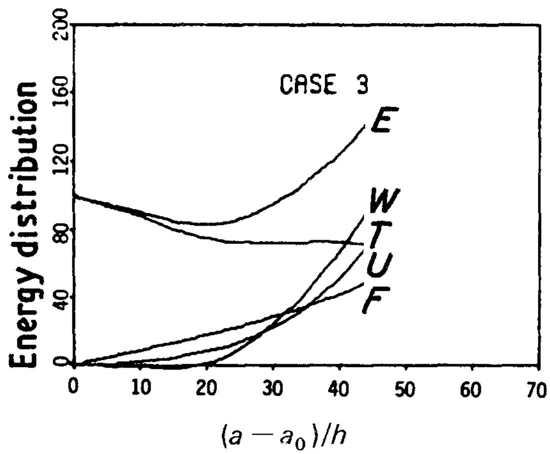

6. Concluding remarks

The results, regarding dynamic crack propagation in the centre-cracked plate specimen, are found to be qualitatively similar to the ones previously reported for the SEN specimen:

(a) The smaller the initial crack length is the larger the following dynamic parameters become: the crack acceleration; the dynamic stress intensity factor; the energy rate; and the absolute and relative kinetic energy.

(b) The dynamic stress intensity factor and the dynamic energy release rate are directly proportional to the initial stress intensity factor K_{Iq}, and its square respectively.

(c) The dynamic stress intensity factor and the energy release rate are considerably influenced by both the geometry and the loading conditions, and are not a unique function of the crack velocity. Hence, it seems that at least in this case, these two parameters in themselves, do not constitute the fracture criterion.

Apart from these similarities some differences between the two configurations can be noticed:

(d) The energy stored in half a CCP specimen at initiation, as anticipated, is higher than that accumulated in an identical SEN specimen. The ratio of the energies varies between 1.03–1.30 for initial cracks of $a_0/W = 0.3$–0.107 respectively.

(e) The fracture energy F and the kinetic energy T in the SEN specimen are built due to the initial strain energy, while in the CCP specimen, their main source is W, the work carried out by the external tractions.

(f) The amount of kinetic energy built up in the CCP specimen is five times higher than the one in the SEN case.

References

1. M. PERL, M. SHMUELY and A. A. BETSER, *Eng. Frac. Mech.* **14** (1981) 142.
2. M. SHMUELY and M. PERL, *ASTM STP* **711** (1980) 54.
3. M. PERL, PhD thesis, Technion – Israel Institute of Technology (1979).
4. A. S. DAY, *Eng.* **219** (1965) 218.
5. M. PERL, *Israel J. Technol.* **20** (1982) 259.
6. M. ISIDA, *ibid.* **7** (1971) 3.
7. A. S. KOBAYASHI and W. L. ENGSTROM, ONR report 064-478 (3A) (1967).
8. A. K. GREEN and P. L. PRATT, *Eng. Frac. Mech.* **6** (1974) 71.
9. M. PERL, *Eng. Fract. Mech.* **15** (1981) 237.

Received 21 October and accepted 25 October 1984